PROCEEDINGS, 51st Workshop on Geothermal Reservoir Engineering
Stanford University, Stanford, California, February 9-11, 2026
SGP-TR-230

# From Oilfield Byproduct to Energy Resource: Decline Curve and LSTM Forecasting of Produced Hot Water in the Bakken Formation (Alger Field).

Emmanuel Agyei[1*], Nathaniel N. Yeboah[1,2], Emmanuel Gyimah[3], Hamid Rahnema[1], William Ampomah[1,2], Benedicta Vidzro[1,2], Kojo Acheampong Boateng[1], Audrey Ayensigna[1], Godsway Akpabli[1]

[1]Petroleum Engineering Department, New Mexico Institute of Mining and Technology, Socorro, New Mexico, USA

[2]Petroleum Recovery Research Center (PRRC), Socorro, New Mexico, USA

[3]New Mexico Bureau of Geology and Mineral Resources, Socorro, New Mexico, USA

[*]E-mail address: emmanuel.agyei@student.nmt.edu

**Keywords:** Decline curve analysis, Geothermal energy potential, Long Short-Term Memory

## ABSTRACT

Produced water, often co-produced with oil and gas, is typically hot and can serve as a valuable geothermal resource for generating energy to support field operations or supply nearby communities and industries. Like hydrocarbon production, the volumetric rate of produced hot water declines with time, making it essential to understand its decline behavior if it is to be harnessed as a sustainable alternative energy source. In this study, production data from three wells, Anderson 28-33 1-H, Charlie Sorenson 17-8 3TFH, and Ross 7-17H, located in the Mississippian/Devonian Bakken formation (Alger field), spanning August 2009 to August 2025, were analyzed to characterize water-production decline trends. The classical Arps decline models (exponential, hyperbolic, and harmonic) and post-Arps models (LGM, SEPD, PLE, Wang model, Duong model, and VDMA) were first employed to evaluate the decline performance of the produced water. The best-performing Arps and post-Arps models for each well were selected and further compared against an LSTM architecture trained on the same historical dataset. The study results showed that, for historical water production data with very little to no fluctuations, empirical DCA models performed equally well as the data-driven LSTM model. However, in instances where production data is severely noisy due to field operations, the data-driven LSTM outperforms the empirical DCA models, both qualitatively and quantitatively. Despite the improved predictive ability of the LSTM model in capturing non-linear dependencies inherent in field data, compared to empirical decline curve analysis models, the mean predictive errors were within 10 - 15%. This error could be further reduced by integrating variables such as well shut-ins, operational interventions, changes in choke settings, artificial lift adjustments, workover activities, water breakthrough events, reservoir pressure variations, and production constraints into the dataset used for training the LSTM model. Including these factors would enable the LSTM model to better distinguish between transient operational effects and underlying reservoir-driven decline behavior.

## 1. INTRODUCTION

Produced water, i.e., the in-situ formation water brought to the surface during oil and gas extraction, is the largest-volume byproduct of hydrocarbon production (Neff et al., 2011). Historically regarded as a waste stream requiring handling, disposal, or reinjection, produced water has more recently gained attention for its potential value in several secondary applications (Cooper et al., 2022; Eyitayo et al., 2023). The most common secondary uses of produced water include reinjection for enhanced oil recovery (Cooper et al., 2022), hydraulic fracturing (EPA, 2011), drilling and completion operations (Reynolds, 2003), limited agricultural applications following strict treatment (Dolan et al., 2018; Sedlacko et al., 2019), and various industrial uses such as cooling, dust suppression, and construction (Farnan et al., 2024; Veil, 2011). These conventional pathways dominate because they align well with existing oilfield infrastructure.

Beyond these traditional uses, produced water also carries significant thermal energy, particularly in reservoirs where formation water temperatures commonly range between ~80-90 °C, and can be even higher (~120 °C) in certain basins (Gong et al., 2011; Liu et al., 2018). This has catalyzed a growing interest in the concept of coproduced geothermal energy, whereby the heat content of produced water is harnessed either for direct-use applications, such as heating greenhouses, aquaculture, and industrial preheating or, when temperatures are sufficient, for power generation using binary cycle or Organic Rankine Cycle technologies (Johnson & Walker, 2010; Reinhardt et al., 2011). Furthermore, several pilot projects have demonstrated that meaningful quantities of electricity can be produced from hot water already being pumped to the surface (Gong et al., 2011; Limpasurat, 2010). However, the technical and economic viability of these systems is strongly influenced by water temperature, flow rate, chemistry, and the overall production lifecycle of the field. While produced water may be used simultaneously for geothermal heat extraction and other oilfield purposes, such dual use depends on the thermal load extracted, regulatory allowances, water quality management, and compatibility with downstream operations.

In the context of harnessing produced water as a geothermal resource, it is worth noting that geothermal energy is widely regarded as a sustainable and low-carbon resource. Therefore, the sustainability of produced water as a geothermal feedstock, which requires understanding how long such a thermal energy source remains available, needs to be thoroughly evaluated in targeted coproduced oil and gas fields (C. E. Clark et al., 2011; Jamil et al., 2024). Importantly, because produced water volumes are directly tied to hydrocarbon reservoir performance, its availability declines as oil and gas production matures (Veil et al., 2004). This further supports that the decline behavior of coproduced geothermal water must be thoroughly characterized to assess long-term resource potential. Encouragingly, the oil

and gas sector has developed a sophisticated toolkit for modeling production declines. Therefore, next-generation geothermal systems can benefit substantially from leveraging knowledge of the hydrocarbon industry, technologies, and analytical frameworks to better understand the sustainability and decline behavior of produced water. Such knowledge and technology adoption between the geothermal and oil and gas factions is currently being championed by the GEODE consortium (Taverna & Leveille, 2025).

For the past decades, production decline in geologic formations has been modeled mainly using empirical and analytical models such as Arp's classical equations (Arps, 1945) and later extensions that incorporates formation type, presence of fractures, boundary-dominated and transient flow regimes (A. J. Clark, 2011; Duong, 2010; Gupta et al., 2018; Ilk et al., 2008; Valkó & Lee, 2010; Wang et al., 2017). Although these methods have been successful, their accuracy is constrained by their individual limitations and assumptions they impose, such as boundary or transient-dominated flow, reservoir flow regimes, and quality of dataset (Vega-Ortiz et al., 2023). Additionally, real field data often exhibit noise, abrupt fluctuations due to operational changes, shut-ins, artificial lift adjustments, varying reservoir pressures, water breakthrough effects, and measurement inconsistencies. These complexities fundamentally characterize the decline behavior of produced fluids as a time series curve fitting and forecasting problem and therefore limit the predictive capability of traditional decline curve models, which struggle to fully capture the nonlinear and time-dependent behavior inherent in produced water systems (Vega-Ortiz et al., 2023).

With the emergence of machine learning, new data-driven approaches have shown strong potential to overcome these time series curve-fitting limitations. Methods such as DeepAR, Prophet analysis, Recurrent Neural Network, Gated Recurrent Unit, Long Short Term Memory, Extreme Gradient Boosting, etc., have been successfully applied to oil and gas decline forecasting in recent literature (Li & Han, 2017; Masini et al., 2019; Tadjer et al., 2021; Vega-Ortiz et al., 2023; Raslan et al., 2026). Among these, the Long Short-Term Memory neural network has gained prominence for its ability to demonstrate attributes (learn temporal dependencies, handle noisy time-series data, accommodate nonlinear trends, and adapt to changes in system behavior) that directly address the shortcomings of empirical models, and the irregularities present in field production data (Vega-Ortiz et al., 2023). LSTM networks outperform many other time-series forecasting models because they are specifically designed to remember long-range temporal patterns by using gated memory cells that prevent information decay (Krichen & Mihoub, 2025). LSTMs adaptively learn nonlinear dependencies and handle irregular, noisy, or highly fluctuating data more effectively.

Building on these insights, the present study investigates the feasibility of using LSTM to model and forecast the decline behavior of produced hot geothermal water from the Bakken formation (Alger field). This study sheds light on the need for geothermal-integrated DCA frameworks in geothermal coproduction. Additionally, this work demonstrates how machine learning can augment and extend classical decline analysis techniques by applying data-driven forecasting to coproduced geothermal water. It also supports the broader strategy of integrating oil and gas expertise into the development of next-generation geothermal energy resources.

## 2. REVIEW OF DECLINE CURVE ANALYSIS MODELS

Decline curve models adopted and analyzed in this study are briefly discussed in this section. These models include the classical Arps models (Arps, 1945), Power Law Exponential (PLE) decline model (Ilk et al., 2008), Stretched Exponential Production Decline (SEPD) model (Valkó & Lee, 2010), Duong model (Duong, 2010), Wang model (Wang et al., 2017), Variable Decline Modified Arps (VDMA) model (Gupta et al., 2018), Logistic Growth Model (LGM) (Clark, 2011), and LSTM for decline curve analysis.

### 2.1 Classical Arps Models

The exponential, hyperbolic, and harmonic decline Arps models were founded on the premise that future well performance will follow the same mathematical trend exhibited in its past production history. This foundation assumes that production rate, time, cumulative output, and decline percentage follow reproducible functional relationships and that these relationships, once identified, may be reliably extrapolated. Additionally, all three Arp's models assume a boundary-dominated flow regime and a near-constant bottom hole pressure and skin coefficient (Tang et al., 2021). Analytically, the exponential, hyperbolic, and harmonic decline models can be represented by **Equations 1**, **2,** and **3**, respectively, where $q_i$, $D_i$, and $b$ are the initial rate of production, decline rate, and decline exponent, respectively. The decline exponent, $b$, assumes values of $0 \leq b \leq 1$, depending on the nature of the production decline.

$$q = q_i e^{-D_i t} \tag{1}$$

$$q = \frac{q_i}{(1 + bD_i t)^{\frac{1}{b}}} \tag{2}$$

$$q = \frac{q_i}{(1 + D_i t)} \tag{3}$$

### 2.2 Power Law Exponent Model (PLE)

PLE model (**Equation 4**), as proposed by Ilk et al. (2008), characterizes production behavior using a decline rate that evolves with time (**Equation 5**). $D_\infty$ represents the long-term decline rate at very large production times, and it is typically treated as a constant for shale gas systems. The parameter $n$ governs how the decline rate shifts over time. This model is also known to be suitable for low-permeability gas shales.

$$q = q_i e^{\left(-D_\infty t - \frac{-D_i}{n} t^n\right)} \tag{4}$$

$$D = D_\infty + D_i t^{-(1-n)} \tag{5}$$

### 2.3 Stretched Exponential Production Decline Model (SEPD)

SEPD was developed using production data from ~7000 Barnett shale wells. This model was designed to capture the extended, nearly flat terminal decline characteristic of shale gas wells. According to (Valkó & Lee, 2010), the decline rate of systems that behave similarly to the final stage of shale gas production can be tracked using **Equation 6**. $\tau$ and $n$ are both empirical constants.

$$q = q_i e^{-\left(\frac{t}{\tau}\right)^n} \tag{6}$$

### 2.4 Duong Model

Duong (2010) formulated the empirical decline curve model (**Equation 7**) for both linear and bilinear fracture-flow regimes. This empirical model is premised on the idea that shale gas wells typically exhibit prolonged fracture-dominated linear flow. $a$ and $m$ are empirical constant tuning parameters. Duong (2010) recommends an $m > 1$. However, for this study, all parameters are optimized with Excel Solver to get values that yield the minimum mean prediction errors of our chosen wells.

$$q = q_i t^{-m} e^{\left(\frac{a}{1-m}\right)(t^{1-m}-1)} \tag{7}$$

### 2.5 Wang Model

Wang et al. (2017) extended fracture-dominated linear flow decline analysis by incorporating a time-dependent index. This decline curve model bridges features of both the stretched exponential and Duong decline curve models (**Equation 8**). $\lambda$ and $n$ are both empirical constants. Though Wang et al. (2017) recommend $n$ to be 2 based on production data from shale gas wells, an optimized value of $n$ and $\lambda$ is estimated for the purpose of applying this model for geothermal coproduction in other oil and gas fields.

$$q = q_i e^{-\lambda(lnt)^n} \tag{8}$$

### 2.6 Variable Decline Modified Arps Model

Gupta et al. (2018) modified the classical Arps models to incorporate a time-dependent decline rate. Rather than assuming a constant decline parameter, the VDMA model applies a power-law form to capture the progressive change in decline behavior with production time (**Equation 9**). $a$ is the decline index governing how rapidly the decline rate evolves.

$$q = q_i e^{-D_i t^{1-a}} \tag{9}$$

### 2.7 Logistic Growth Model

Clark (2011) adapted logistic growth model, which was originally developed for population dynamics, to forecast the production of shale gas wells. The variant of LGM suited for decline curve analysis contains a carrying capacity term, *K*, a hyperbolic exponent, *n*, and an empirical constant, *a* (**Equation 10**). In original terms, the carrying capacity denotes the overall hydrocarbon volumes that the well can produce to the surface by depending only on primary recovery. The empirical constant, *a*, also reflects the time exponent *n* that needs to elapse for half of the carrying capacity to be brought to the surface. For this study, we will define the carrying capacity as the amount of geothermal water the individual wells can produce by using the natural energy of the reservoir.

$$q = \frac{Knat^{(n-1)}}{(a+t^n)^2} \tag{10}$$

### 2.8 LSTM Decline Forecasting Model

Long Short-Term Memory networks are a specialized class of recurrent neural networks designed for forecasting sequential data by capturing long-range temporal dependencies that conventional RNNs cannot sustain due mainly to vanishing or exploding gradients. An LSTM unit incorporates gating mechanisms, such as input, forget, and output gates, that regulate information flow through a persistent cell state $c_t$. This enables robust learning of nonlinear, time-dependent production trends. In this study, each LSTM decline model employs a stacked architecture designed to capture both short and medium-term temporal dependencies. The network consists of (a) a first LSTM layer with 64 hidden units and sequence output enabled, (b) a dropout layer for regularization, (c) a second LSTM layer with 32 hidden units, (d) a second dropout layer, and (d) a fully connected output layer producing a single scalar prediction. The LSTM updates follow the standard gated formulations (**Equation 11 – 16**), which enable it to learn dynamic decline patterns, noise characteristics, and nonlinear dependencies in production data. **Figure 1** also shows the schematic of a basic LSTM model.

$$f_t = \sigma\left(W_f[h_{t-1}, x_t] + b_f\right) \tag{11}$$

$$\tilde{C}_t = tanh(W_c[h_{t-1}, x_t] + b_c) \tag{12}$$

$$i_t = \sigma(W_i[h_{t-1}, x_t] + b_i) \tag{13}$$

$$o_t = \sigma(W_o[h_{t-1}, x_t] + b_o) \tag{14}$$

$$c_t = f_t \odot c_{t-1} + i_t \odot \tilde{C}_t \tag{15}$$

$$h_t = o_t \odot \tanh(c_t) \tag{16}$$

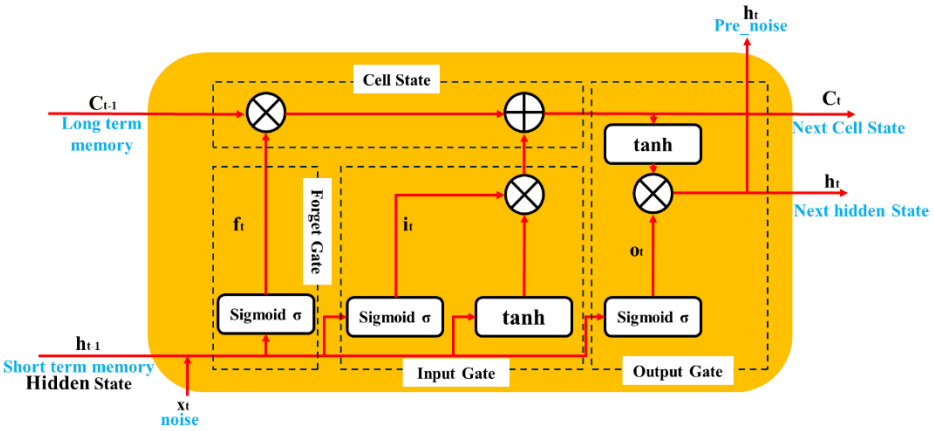


**Figure 1: Basic Schematic of how an LSTM model arrives at predictions.**

## 3. METHODOLOGY

### 3.1 Data Collection and Pre-Processing

A consolidated dataset of cogeothermal water production was obtained from three wells, namely, Anderson 2833 1-H, Charlie Sorenson 17-8 3TFHP, and Ross 7-17 H, completed in the Mississippian/Devonian Bakken formation (Alger field) and covering the period from August 2009 to September 2025 (**Figure 2** shows raw datasets). To preserve the inherent variability and operational noise characteristic of real field performance, the Anderson 2833 1-H dataset was intentionally left unprocessed. For the other two wells, months with no recorded production were removed from the dataset. However, when zero-production months occurred within otherwise productive years, those entries were estimated using the mean monthly water production and corresponding time value to maintain temporal continuity. Monthly water volumes were converted to flow rates by dividing by the number of days over which the reported cumulative volume was produced. Such preprocessing was necessary to ensure temporal consistency, reduce discontinuities, and prevent artificial gaps or noise from biasing parameter estimation and predictive performance of models. **Figure 3** shows the preprocessed dataset used for the decline curve analysis. For LSTM decline modelling, further data preprocessing, such as normalization and supervised sequence construction, was required.

#### 3.1.1 Normalization

To stabilize training and ensure numerical consistency of the LSTM decline model, the production rate series was normalized using min–max scaling (**Equation 17**), where $q_{\min}$ and $q_{\max}$ are the minimum and maximum observed water production rates in the dataset, respectively. All LSTM modeling was performed in the normalized space, and predictions were subsequently transformed back to physical units.

$$\widetilde{q_t} = \frac{q_t - q_{min}}{q_{max} - q_{min}} \tag{17}$$

#### 3.1.2 Supervised Sequence Construction

The LSTM time series was reformulated as a supervised learning problem using a sliding window approach. For a given look-back window $L$, input–output pairs were defined using conditions presented in **Equation 18**. This formulation allowed the LSTM to infer $q_t$ from the preceding $L$ months of production history. In this work, four values of $L$ (1,3,6,and 12 months) were adopted. The best-performing look-back window was selected for further comparison.

$$x_t = [\tilde{q}_{t-L},\ \tilde{q}_{t-L+1}, \ldots, \tilde{q}_{t-1}],\ y_t = \widetilde{q_t}, for\ t = L+1, \ldots, T \tag{18}$$

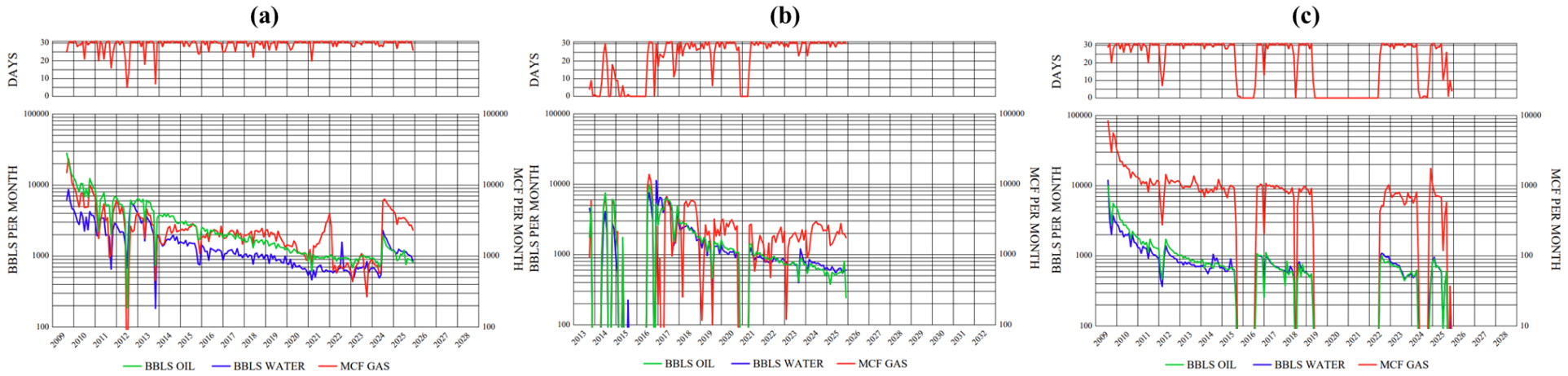


**Figure 2: Raw geothermal water production rates from (a) Anderson 2833 1-H, (b) Charlie Sorenson 17-8 3TFHP, and (c) Ross 7-17 H production wells in the Bakken formation (Alger field) (North Dakota Department of Mineral Resources, 2025).**

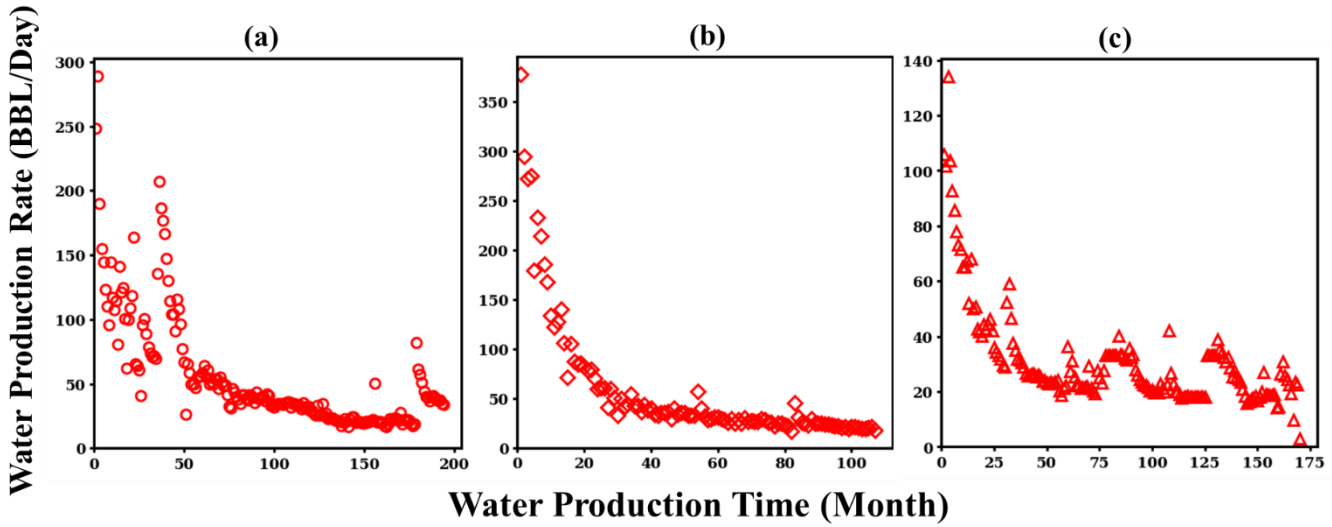


**Figure 3: Cleaned geothermal water production rates from (a) Anderson 2833 1-H, (b) Charlie Sorenson 17-8 3TFHP, and (c) Ross 7-17 H production wells in the Bakken formation (Alger field).**

### 3.2 Decline Curve Modelling

The preprocessed datasets were subsequently used to construct decline curves using all seven empirical formulations. This step enabled a comprehensive evaluation of decline behavior across the three wells in the Bakken Formation (Alger field). Empirical parameter estimation for each model, including decline rates, characteristic time constants, hyperbolic and stretching exponents, and other model-specific coefficients, was estimated using Excel's optimization framework, where model constants were tuned to minimize the mean prediction error between observed and modeled production. Owing to their foundational role in decline-curve analysis, the Arps formulations were treated separately from the newer empirical models. This allowed their exponential, hyperbolic, and harmonic behaviors to be assessed independently. From this suite of empirical evaluations, the best-performing Arps model and the leading non-Arps model were selected for direct comparison against the data-driven LSTM forecasting approach.

For the LSTM-based decline analysis, the preprocessed data were partitioned into training and testing sets using an 80/20 split, normalized to stabilize learning, and subsequently used to train a sequence-to-sequence forecasting model for benchmarking against the empirical decline-curve predictions. To preserve temporal causality, the dataset is partitioned chronologically rather than randomly. The first 80% of the available supervised samples were used for training, while the remaining 20% were reserved for out-of-sample testing. Additionally, all LSTM models were trained using the Adam optimizer to minimize the mean squared error (MSE).

#### 3.2.1 Error Metrics

The accuracy of the empirical and data-driven predictions was quantified using the mean absolute error, mean absolute percentage error (MAPE), and the root mean square error (RMSE). MAPE measures the average relative deviation between predicted and observed values as defined in **Equation 19,** while RMSE evaluates the magnitude of absolute prediction errors and is given by **Equation 20**. To further understand the behavior of model inaccuracies throughout the decline process, error distributions for all models were visualized using histograms. This allowed identification of specific regions, early-time transients, mid-life transition zones, or late-time tail behavior, where prediction errors were most pronounced, thereby providing additional diagnostic insights beyond aggregate error metrics. $q_a$, $\widehat{q_p}$ and N are the actual well flow rate, predicted flow rate by models, and total number of recorded datapoints of each well, respectively.

$$MAPE = \frac{100}{N}\sum_{I=1}^{N}\left|\frac{q_a - \widehat{q_p}}{q_a}\right| \tag{19}$$

$$RMSE = \sqrt{\frac{1}{N}\sum_{I=1}^{N}\left(q_a - \widehat{q_p}\right)^2} \tag{20}$$

## 4. RESULTS AND DISCUSSION

### 4.1 Decline Curve Analysis of Classical Arps Models

**Figure 4(a–c)** illustrates the performance of the classical Arps decline models: exponential, hyperbolic, and harmonic, when applied to the three wells under study. Each model was calibrated using Excel's nonlinear optimization to identify the decline parameters that minimized absolute percentage error, including both the nominal decline rate, $D_i$, for all models and the hyperbolic exponent, $b$, for the hyperbolic case. For Charlie Sor. 17-8 3TFHP well, where the cleaned production data exhibited minimal noise and consistent downward trends, both the hyperbolic and harmonic models reproduced the qualitative trajectory of the decline. Quantitatively, the harmonic model provided the most accurate overall fit and achieved an MAPE of 12.2% and an MSE of 14.3 BBL/month, while the hyperbolic model performed comparably with a MAPE of 12.4% and an MSE of 14.4 BBL/month.

In contrast, the Anderson 2833 1-H and Ross 7-17 H wells displayed substantial disturbances in their water-production time series, arising from possible operational and reservoir-related effects such as intermittent choke adjustments, transient water breakthrough, offset-well interference, workovers, or pressure perturbations induced by nearby water injection. These features introduced large deviations from monotonic decline and resulted in poor quantitative performance for all Arps models. Although hyperbolic and harmonic curves qualitatively followed the general decreasing trend in Anderson 2833 1-H well, they failed to capture abrupt excursions in the data, and therefore, produced localized errors exceeding 100% in intervals dominated by noise. The Ross 7-17H well posed an even greater challenge. Despite data cleaning, the production record remained dominated by erratic variations. This hindered any of the Arps models from matching the observed decline either qualitatively or quantitatively. These outcomes emphasize the sensitivity of empirical decline-curve models to deviations from stable boundary-dominated flow and highlight the limitations of Arps-based forecasting in environments where field activities or reservoir phenomena obscure the underlying decline signal.

Across all three wells, the harmonic model consistently outperformed the exponential and hyperbolic models and offered the most stable behavior in both low-noise and moderately noisy data conditions. Because of this superior performance and its ability to capture the curvature observed in unconventional decline without imposing the restrictive constant-decline assumption of the exponential model, the harmonic formulation was selected as the reference decline-curve model for comparison against the long-short-term-memory (LSTM) time-series forecasting approach. Performance of all three models across all three wells is presented in **Table 1**.

**Table 1: Metrics from decline curve analysis using the Arps models.**

| Current well name | Arps model | Decline rate ($D_i$) | Hyperbolic Exponent (b) | RMSE | MAPE (%) |
|---|---|---|---|---|---|
| Anderson 28-33 1-H | Exponential | 0.0183 | - | 38.1 | 42.8 |
| | Hyperbolic | 0.0641 | 0.99 | 26.4 | 21.1 |
| | Harmonic | 0.0641 | 1 | 26.3 | 21.1 |
| Charlie S. 17-8 3TFH | Exponential | 0.0559 | - | 31.8 | 58.3 |
| | Hyperbolic | 0.1871 | 0.99 | 14.4 | 12.4 |
| | Harmonic | 0.1871 | 1 | 14.3 | 12.3 |
| Ross 7-17H | Exponential | 0.0145 | - | 8.2 | 20.0 |
| | Hyperbolic | 0.0369 | 0.99 | 6.2 | 13.9 |
| | Harmonic | 0.0369 | 1 | 6.2 | 13.8 |

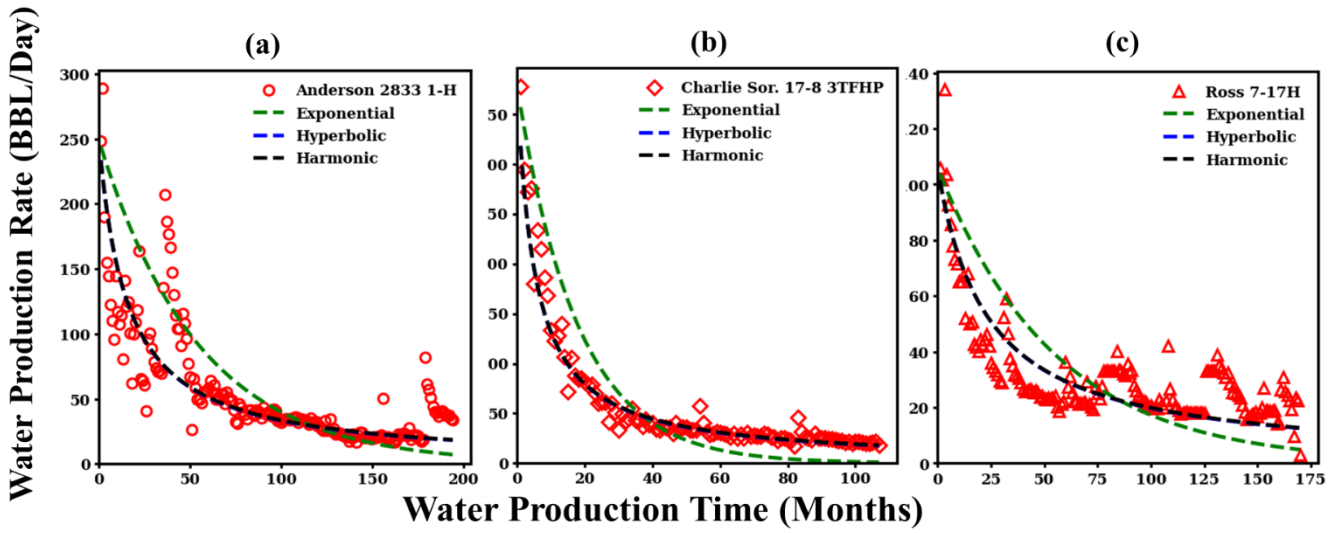


**Figure 4: Classical Arps decline curve fits (exponential, hyperbolic, and harmonic) modeled from historical production data for the (a) Anderson 2833 1-H, (b) Charlie Sor. 17-8 3TFHP, and (c) Ross 7-17H wells.**

### 4.2 Decline Curve Analysis of Post-Arps Models

**Figure 5(a-c)** compares the post-Arps decline models, Power Law Exponential (PLE) (Ilk et al., 2008), Stretched Exponential Production Decline (SEPD) (Valkó & Lee, 2010), Duong model (Duong, 2010), Wang model (Wang et al., 2017), Variable Decline Modified Arps (VDMA) (Gupta et al., 2018), and Logistic Growth Model (LGM) (Clark, 2011), against the production histories of the Charlie Sor. 17-8 3TFHP, Anderson 2833 1-H, and Ross 7-17H wells. Like the classical Arps models, all post-Arps models were affected by the noise present in the datasets, which originates from normal field operations. This sensitivity arises because most post-Arps models remain structural variants of the Arps models. They only modify the functional form of the decline rate, typically by allowing time-dependent effective decline (Wang, VDMA), empirical flow-regime corrections (Duong), stretched or power-law relaxation (SEPD, PLE), or logistic-type saturation behavior (LGM), yet they somewhat rely on the assumption that underlying production follows a smooth, monotonic decline dominated by reservoir physics rather than operational noise. Additionally, these models were originally developed using datasets from systems with extended and well-behaved transient flow regimes, particularly shale gas wells, which typically exhibit strong power-law transient signatures absent or masked in noisier water-production environments.

For Charlie Sor. 17-8 3TFHP well, where the cleaned dataset preserved a clear decline trend with minimal operational distortion, several models matched the qualitative behavior of the decline. The Wang, VDMA, LGM, and Duong models reproduced the curvature of the early-time and mid-time decline because they incorporate mechanisms that mimic a gradual reduction of effective fracture contribution or a transient linear-to-boundary-dominated transition. SEPD, PLE, and VDMA, however, matched the data only beyond month 25 because their formulations assume a prolonged transient flow regime or stretched/power-law decay that is not fully representative of the early-time decline for this well. Quantitatively, the Wang model provided the best fit, achieving an MAPE of 11.1%.

For Anderson 2833 1-H and Ross 7-17H wells, the structural assumptions of the post-Arps models were strongly violated. None of the models were able to produce physically meaningful early time matches for these wells, and all failed to quantitatively predict the decline in regions affected by severe noise, large operational perturbations, or abrupt rate discontinuities. In the Anderson 2833 1-H well, some models were able to mimic the general direction of the decline. For the Ross 7-17H well, the noise overwhelmed the decline signal to the extent that no model, classical Arps or post-Arps, was able to qualitatively or quantitatively match the production behavior. For model selection, the Wang model was chosen for the Charlie Sorenson 17-8 3TFHP well because it achieved the lowest error and provided the most stable representation of the decline. For the Anderson 2833 1-H and Ross 7-17H wells, the Logistic Growth Model (LGM) was selected, as it delivered the best performance (yielded MAPEs of 19.4% and 20.4%, respectively) among the post-Arps models despite the high noise levels in both datasets.

**Table 2: Metrics from decline curve analysis using Post-Arps models.**

| Current well name | Post-Arps model | Empirical constants | MAPE (%) |
|---|---|---|---|
| Anderson 28-33 1-H | PLE (Ilk et al., 2008) | $D_i = 0.569$<br>$D_\infty = 0.0104$<br>$n$ = 0.640 | 21.1 |
| | SEPD (Valkó & Lee, 2010) | $\tau = 22.9$<br>$n$ = 0.464 | 19.6 |
| | Duong model (Duong, 2010) | $m$ = 0.915<br>$a$ = 0.382 | 29.0 |
| | VDMA (Gupta et al., 2018) | $D_i = 0.232$<br>$a$ = 0.535 | 19.6 |
| | Wang model (Wang et al., 2017) | $\lambda = 0.122$<br>$n$ = 1.833 | 20.9 |
| | LGM (Clark, 2011) | $K$ = 14745.8<br>$n$ = 0.942<br>$a$ = 82.9 | 19.4 |
| Charlie S. 17-8 3TFH | PLE (Ilk et al., 2008) | $D_i = 0.788$<br>$D_\infty = 0.012$<br>$n$ = 0.449 | 19.9 |
| | SEPD (Valkó & Lee, 2010) | $\tau = 3.45$<br>$n$ = 0.864 | 14.7 |
| | Duong model (Duong, 2010) | $m$ = 1.2<br>$a$ = 0.864 | 11.3 |
| | VDMA (Gupta et al., 2018) | $D_i = 0.671$<br>$a$ = 0.679 | 14.7 |
| | Wang model (Wang et al., 2017) | $\lambda = 0.399$<br>$n$ = 1.301 | 11.1 |
| | LGM (Clark, 2011) | $K$ = 33563.1<br>$n$ = 0.375<br>$a$ = 21.5 | 11.4 |
| Ross 7-17H | PLE (Ilk et al., 2008) | $D_i = 0.662$<br>$D_\infty = 0.005$<br>$n$ = 0.632 | 24.3 |
| | SEPD (Valkó & Lee, 2010) | $\tau = 19.3$<br>$n$ = 0.298 | 22.0 |
| | Duong model (Duong, 2010) | $m$ = 1.06<br>$a$ = 0.797 | 20.5 |
| | VDMA (Gupta et al., 2018), | $D_i = 0.414$<br>$a$ = 0.702 | 22.0 |
| | Wang model (Wang et al., 2017), | $\lambda = 0.252$<br>$n$ = 1.230 | 20.5 |
| | LGM (Clark, 2011) | $K$ = 3558497.7<br>$n$ = 0.592<br>$a$ = 15578.6 | 20.4 |

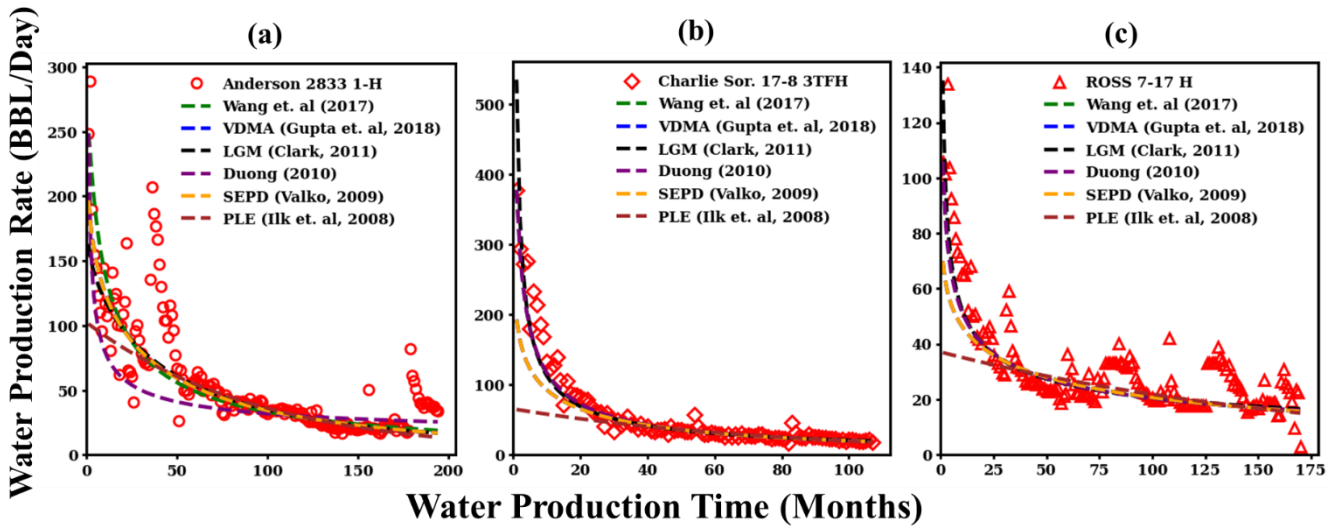


**Figure 5: Post-Arps decline curve fits modeled from historical production data for the (a) Anderson 2833 1-H, (b) Charlie Sor. 17-8 3TFHP, and (c) Ross 7-17H wells.**

### 4.3 LSTM Time Series Decline Analysis

**Figure 6** illustrates the qualitative performance of the four LSTM decline-forecasting models developed using different look-back windows of 1, 3, 6, and 12 months for each well. The look-back window controls the length of historical information available to the network when predicting future production and therefore directly influences the model's ability to capture short-term fluctuations versus longer-term decline structure. Across all wells, clear differences were observed in how effectively each look-back configuration tracks the underlying production trend. For each well, the LSTM configuration that demonstrated the most stable qualitative behavior and superior quantitative accuracy was selected for further comparison with the empirical decline-curve models. **Tables 3–5** summarize the quantitative performance of all LSTM models across the three wells.

For the Ross 7-17H well, the LSTM with a look-back window of 3 months produced the best overall performance, yielding the lowest training and testing MAE values of 3.9 and 4.1, respectively. This result indicates that a relatively short historical memory was sufficient to capture the dominant production dynamics of this well, while longer look-back windows offered no additional predictive benefit and, in some cases, degraded performance due to over-smoothing. In contrast, the Anderson 2833 1-H well benefited from a longer temporal context. The LSTM with a 6-month look-back window achieved the lowest training and testing MAE values of 9.7 and 6.4, respectively, suggesting that incorporating a broader production history improved the model's ability to filter noise and learn the underlying decline behavior. A similar outcome was observed for the Charlie Sorenson 17-8 3TFHP well, where the 6-month look-back LSTM outperformed all other configurations, achieving a training MAE of 7.1 and a testing MAE of 1.1. The very low testing error for this well reflects the relatively smooth production profile and the suitability of a longer memory length for capturing its decline structure.

Based on these results, the LSTM models with look-back windows of 3 months for Ross 7-17H and 6 months for both Anderson 2833 1-H and Charlie Sorenson 17-8 3TFHP were selected for direct comparison with the empirical decline-curve models.

**Table 3: LSTM performance metrics for ROSS 17-7H.**

| look-back period (Months) | train RMSE | train MAE | test RMSE | test MAE |
|---|---|---|---|---|
| 1 | 19.7 | 11.4 | 5.6 | 4.4 |
| 3 | 6.0 | 3.9 | 5.5 | 4.1 |
| 6 | 6.4 | 4.4 | 5.9 | 4.4 |
| 12 | 7.9 | 5.3 | 5.5 | 3.8 |

**Table 4: LSTM performance metrics for Anderson 2833 1-H.**

| look-back period (Months) | train RMSE | train MAE | test RMSE | test MAE |
|---|---|---|---|---|
| 1 | 48.5 | 29.4 | 14.6 | 11.9 |
| 3 | 22.7 | 11.9 | 12.7 | 7.0 |
| 6 | 19.8 | 9.7 | 12.6 | 6.4 |
| 12 | 20.7 | 10.3 | 12.7 | 6.9 |

**Table 5: LSTM performance metrics for Charlie Sorenson 17-8 3TFHP.**

| look-back period (Months) | train RMSE | train MAE | test RMSE | test MAE |
|---|---|---|---|---|
| 1 | 72.3 | 40.6 | 2.6 | 2.1 |
| 3 | 12.9 | 8.1 | 1.7 | 1.2 |
| 6 | 9.8 | 7.1 | 1.4 | 1.1 |
| 12 | 9.8 | 6.9 | 2.1 | 1.7 |

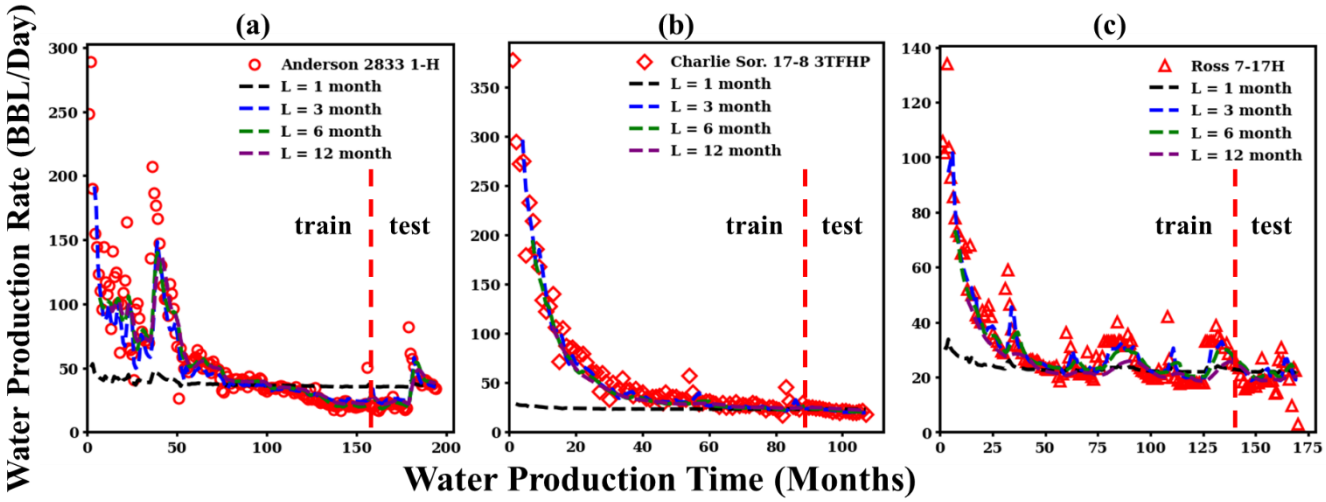


**Figure 6: LSTM decline curve fits modeled from historical production data for the (a) Anderson 2833 1-H, (b) Charlie Sor. 17-8 3TFHP, and (c) Ross 7-17H wells.**

### 4.4 Model Comparisons

**Figure 7** compares the performance of the best-performing LSTM models against the best-performing Arps and post-Arps decline-curve models for the three representative wells. For the Charlie Sorenson 17-8 3TFHP well, which exhibits relatively smooth production behavior, all models demonstrate comparable predictive performance. The LSTM model with a 6-month look-back window achieved an MAPE of 11.6%, the Wang model with 11.1%, and the harmonic decline model with 12.3%. The slightly superior performance of the Wang model relative to the harmonic model can be attributed to its ability to capture time-varying decline behavior through its flexible formulation, which relaxes the constant-decline assumption inherent in the harmonic model. For smooth datasets, this added flexibility provides marginal improvements without introducing overfitting.

In contrast, for the Anderson 2833 1-H and Ross 7-17H wells, which exhibit significant noise and variability representative of most field production datasets, the LSTM models clearly outperform the empirical decline-curve models, both qualitatively and quantitatively. For the Anderson well, the LSTM model achieved a MAPE of 15.2%, compared to 21.1% for the harmonic model and 19.4% for the LGM

model. Similarly, for the Ross well, the LSTM model yielded a MAPE of 13.4%, outperforming the harmonic model (13.8%) and substantially outperforming the LGM model (20.4%).

These results highlight the robustness of the LSTM framework in handling noisy production data, where its data-driven architecture enables it to learn complex, non-linear temporal patterns that are not adequately captured by traditional Arps or post-Arps formulations

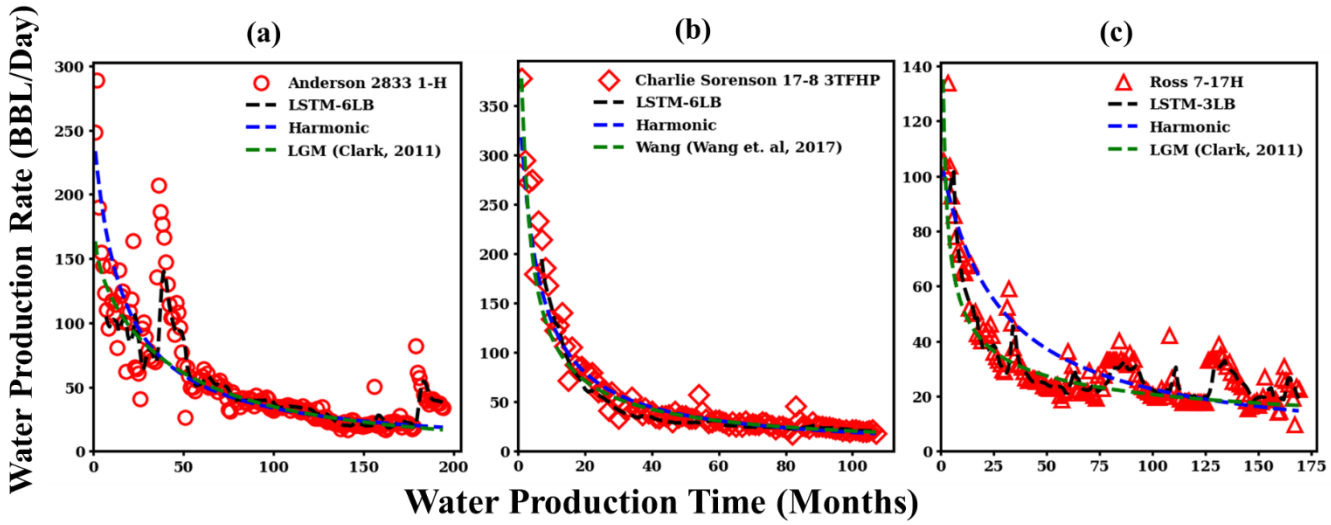


**Figure 7: Data-driven and empirical DCA model comparisons for (a) Anderson 2833 1-H, (b) Charlie Sor. 17-8 3TFHP, and (c) Ross 7-17H wells.**

## CONCLUSION AND RECOMMENDATION

This study successfully demonstrated the superior predictive capability of a data-driven Long Short-Term Memory (LSTM) model over traditional empirical decline-curve models for forecasting the decline behavior of produced water in oil fields. Across wells with varying data characteristics, the LSTM framework consistently provided more accurate predictions, particularly in datasets exhibiting noise and fluctuations that are representative of real-field production conditions. Unlike empirical Arps and post-Arps models, which rely on fixed functional forms and simplifying assumptions, the LSTM model effectively captured complex, non-linear temporal patterns inherent in produced water data.

Despite the demonstrated superiority of the LSTM model, its predictive performance can be further improved by incorporating additional operational and reservoir-related factors that contribute to fluctuations and noise in production data. Future studies should focus on obtaining and integrating variables such as well shut-ins, operational interventions, changes in choke settings, artificial lift adjustments, workover activities, water breakthrough events, reservoir pressure variations, and production constraints into the training dataset. Including these factors would enable the LSTM model to better distinguish between transient operational effects and underlying reservoir-driven decline behavior. Secondly, attempts can be made to combine black-box LSTM models with white-box regression models guided by real physics constraints to generate a grey-box model for more enhanced interpretability.

Furthermore, expanding the framework to incorporate multivariate inputs and real-time field data, as well as evaluating model generalizability across larger well populations, would enhance the robustness and practical deployment of data-driven decline forecasting tools in field-scale reservoir management.

**REFERENCES**

Clark, A. J.: Decline Curve Analysis in Unconventional Resource Plays Using Logistic Growth Models, 116, (2011).

Clark, C. E., Sullivan, J. L., & Wang, M. Q.: Water Use in the Development of Geothermal Power Plants, In ANL/EVS/R-10/5, (2011).

Cooper, C. M., McCall, J., Stokes, S. C., McKay, C., Bentley, M. J., Rosenblum, J. S., Blewett, T. A., Huang, Z., Miara, A., Talmadge, M., Evans, A., Sitterley, K. A., Kurup, P., Stokes-Draut, J. R., Macknick, J., Borch, T., Cath, T. Y., & Katz, L. E.: Oil and Gas Produced Water Reuse: Opportunities, Treatment Needs, and Challenges, ACS ES and T Engineering, 2(3), (2022), 347–366, https://doi.org/10.1021/acsestengg.1c00248

Dolan, F. C., Cath, T. Y., & Hogue, T. S.: Assessing the feasibility of using produced water for irrigation in Colorado, Science of the Total Environment, 640–641, (2018), 619–628, https://doi.org/10.1016/j.scitotenv.2018.05.200

Duong, A. N.: An unconventional rate decline approach for tight and fracture-dominated gas wells, Society of Petroleum Engineers - Canadian Unconventional Resources and International Petroleum Conference 2010, 3(December), 2052–2066, https://doi.org/10.2118/137748-ms

EPA.: Proceedings of the Technical Workshops for the Hydraulic Fracturing Study: Water Resources Management, Environmental Protection Agency, Washington D.C. (2011). May, www.epa.gov

Eyitayo, S. I., Watson, M. C., Kolawole, O., Xu, P., Bruant, R., & Henthorne, L.: Produced Water Treatment: Review of Technological Advancement in Hydrocarbon Recovery Processes, Well Stimulation, and Permanent Disposal Wells. SPE Production and Operations, 38(1), (2023), 51–62, https://doi.org/10.2118/212275-PA

Farnan, J., Eck, A., Kearney, A., Dorman, F. L., Ismail, H., Chase, E., Liu, X., Warner, N. R., & Burgos, W. D.: Oil and gas produced waters fail to meet beneficial reuse recommendations for use as dust suppressants, Science of the Total Environment, (2024), 919(January), 170807, https://doi.org/10.1016/j.scitotenv.2024.170807

Gong, B., Liang, H., Xin, S., & Li, K.: Effect of Water Injection on Reservoir Temperature During Power Generation in Oil Fields, PROCEEDINGS, Thirty-Sixth Workshop on Geothermal Reservoir Engineering, 2007.

Gupta, I., Rai, C., Sondergeld, C., & Devegowda, D.: Variable exponential decline: Modified ArPs to characterize unconventional-shale production performance, SPE Reservoir Evaluation and Engineering, 21(4), (2018), 1045–1057, https://doi.org/10.2118/194005-PA

Ilk, D., Rushing, J. A., Perego, A. D., & Blasingame, T. A.: Exponential vs. hyperbolic decline in tight gas sands -understanding the origin and implications for reserve estimates using arps' decline curves, Proceedings - SPE Annual Technical Conference and Exhibition, 7(December), (2008), 4637–4659, https://doi.org/10.2118/116731-ms

Jamil, F., Shafiq, I., Sarwer, A., Ahmad, M., Akhter, P., Inayat, A., Shafique, S., Park, Y. K., & Hussain, M.: A critical review on the effective utilization of geothermal energy, Energy and Environment, 35(1), (2024), 438–457, https://doi.org/10.1177/0958305X231153969

JJ. Arps.: Chapter II . Petroleum Economics (Decline curves), Transactions of the AIME, 160(01), (1945), 228–247, https://petrowiki.spe.org/Types_of_decline_analysis_in_production_forecasting%0Ahttps://onepetro.org/TRANS/article/160/01/228/161823/Analysis-of-Decline-Curves

Johnson, L., & Walker, E.: Ormat : Low-Temperature Geothermal Power Generation, 083(3), (2010).

Krichen, M., & Mihoub, A.: Long Short-Term Memory Networks: A Comprehensive Survey, AI (Switzerland), 6(9), (2025), 1–21, https://doi.org/10.3390/ai6090215.

Li, Y., & Han, Y.: Decline curve analysis for production forecasting based on machine learning, Society of Petroleum Engineers - SPE Symposium: Production Enhancement and Cost Optimisation 2017, December 2025, 1–14, https://doi.org/10.2118/189205-ms.

Limpasurat, A.: Reservoirs, Artificial Geothermal Energy Potential of Steam-Flooded Heavy Oil, (Issue August), (2010).

Liu, X., Falcone, G., & Alimonti, C.: A systematic study of harnessing low-temperature geothermal energy from oil and gas reservoirs, Energy, 142, (2018), 346–355. https://doi.org/10.1016/j.energy.2017.10.058.

Masini, S. R., Goswami, S., Kumar, A., & Balaji, C.: Decline Curve Analysis Using Artificial Intelligence, ペインクリニック学会治療指針２, (2019), 1–9.

Neff, J., Lee, K., & DeBlois, E. M.: Produced Water: Overview of Composition, Fates, and Effects, Produced Water, (2011), 3–54, https://doi.org/10.1007/978-1-4614-0046-2_1

North Dakota Department of Mineral Resources, Oil & Gas Division.: *NDGS Core Library Search*. Retrieved October 2, 2025, from https://www.dmr.nd.gov/oilgas/feeservices/findcores.asp

Raslan, K., Elnaggar, H., Shahin, A., Owusu, I., Elagab, O., Aboushanab, M., Sobhy, M., Nafea, B. and Adam, A.: Real-Time Estimation of Production Rates in Gas Condensate Wells Using a Machine Learning Model. In International Petroleum Technology Conference, (2026, January), (p. D021S010R007). IPTC.

Reinhardt, T., Johnson, L., & Popovich, N.: Systems for Electrical Power from Coproduced and Low Temperature Geothermal Resources, Thirty-Sixth Workshop on Geothermal Reservoir Engineering, (2011), 5, https://gondwana.stanford.edu/ERE/pdf/IGAstandard/SGW/2011/reinhardt.pdf.

Reynolds, R.R. and Kiker, R.D.: Produced water and associated issues, *Oklahoma Geological Survey*, (2003).

Sedlacko, E. M., Jahn, C. E., Heuberger, A. L., Sindt, N. M., Miller, H. M., Borch, T., Blaine, A. C., Cath, T. Y., & Higgins, C. P.: Potential for Beneficial Reuse of Oil and Gas–Derived Produced Water in Agriculture: Physiological and Morphological Responses in Spring Wheat (Triticum aestivum), Environmental Toxicology and Chemistry, 38(8), (2019), 1756–1769, https://doi.org/10.1002/etc.4449.

Tadjer, A., Hong, A., & Bratvold, R. B.: Machine learning based decline curve analysis for short-term oil production forecast, Energy Exploration and Exploitation, 39(5), (2021), 1747–1769, https://doi.org/10.1177/01445987211011784.

Tang, H., Zhang, B., Liu, S., Li, H., Huo, D., & Wu, Y. S.: A novel decline curve regression procedure for analyzing shale gas production, Journal of Natural Gas Science and Engineering, 88(January), (2021), https://doi.org/10.1016/j.jngse.2021.103818.

Taverna, N., & Leveille, G.: Data Sharing as a Catalyst for Expanding the Energy Frontier, SPE Western Regional Meeting Proceedings, 2025-April(December), (2025), 1–12, https://doi.org/10.2118/224199-MS.

Valkó, P. P., & Lee, W. J.: A better way to forecast production from unconventional gas wells, Proceedings - SPE Annual Technical Conference and Exhibition, 3(September 2010), (2010), 1860–1875, https://doi.org/10.2118/134231-ms.

Vega-Ortiz, C., Panja, P., Deo, M., & McPherson, B., Decline Curve Analysis using Machine Learning Algorithms: RNN, LSTM, and GRU. 57th US Rock Mechanics/Geomechanics Symposium, December. (2023), https://doi.org/10.56952/ARMA-2023-0287.

Veil, J. A.: Produced Water Management Options and Technologies, In Produced Water, (2011), https://doi.org/10.1007/978-1-4614-0046-2_29

Veil, J. A., Puder, M. G., Elcock, D., & Redweik, R. J. Jr.: A White Paper Describing Produced Water from Production of Crude Oil, Natural Gas, and Coal Bed Methane, Prepared by: Argonne National Laboratory, Prepared for: U.S. Department of Energy National Energy Technology Laboratory Under Contract W-31-109-Eng-38, In Argonne National Laboratory report, prepare for U.S Department of Energy and National Energy Technology laboratory (Issue January), http://www.osti.gov/servlets/purl/821666/%0Ahttp://www.circleofblue.org/waternews/wp-content/uploads/2010/08/prodwaterpaper1.pdf, (2004).

Wang, K., Li, H., Wang, J., Jiang, B., Bu, C., Zhang, Q., & Luo, W.: Predicting production and estimated ultimate recoveries for shale gas wells: A new methodology approach, Applied Energy, 206(July), (2017), 1416–1431. https://doi.org/10.1016/j.apenergy.2017.09.119